Rayleigh scattering from excited states of atoms and ions

J. P. J. Carney and R. H. Pratt
Department of Physics and Astronomy, University of Pittsburgh, Pittsburgh, Pennsylvania 15260

Lynn Kissel*
Physics and Space Technology, Lawrence Livermore National Laboratory, Livermore, California 94551-0808

S. C. Roy
Department of Physics, Bose Institute, Calcutta 700009, West Bengal, India

S. K. Sen Gupta
University Science Instrumentation Centre, North Bengal University, Darjeeling 734430, India
(Received 12 August 1999; revised manuscript received 21 December 1999; published 13 April 2000)

Elastic photon scattering from the ground state and various excited states of carbon atoms and ions has been investigated, using the *S*-matrix formalism, for incident photon energies ranging from 100 eV to 10 keV, contrasting the results obtained for different configurations. The excited states considered include hollow-atom states, where one or more inner shells are completely vacated. Ionic cases are considered as a limit of excitation. Results demonstrate how cross sections for different excited states group together according to shared properties of the configurations, such as the number of *K* electrons. Cross sections may exhibit deep dips below the *K* edge, depending on the occupation of the subshells corresponding to the strongest transitions. Scattering from excited states can have significantly larger cross sections than scattering from the ground state, particularly just below the *K* resonance region, and therefore it needs to be considered in situations where there is a large population of these excited states. Results are interpreted in terms of form-factor arguments and the qualitative behavior of individual subshell amplitudes. The angular dependence of cross sections can be understood in terms of angle-dependent form factors and anomalous scattering factors, taken to be angle independent. Cases are identified for which excited-state total integrated cross sections are much larger than the corresponding cross sections for scattering from the ground state. Our main results use an averaging over magnetic substates at the level of the amplitude, exact only for fully filled subshells, but generally appropriate for the carbon case considered, which simplifies the discussion and explains most of the general features. We also present results for a hollow lithium atom with and without this approximation to illustrate the differences that can arise in certain circumstances.

PACS number(s): 32.80.Cy, 31.50.+w

I. INTRODUCTION

There exists an extensive literature on the elastic scattering of x rays by atoms in their ground states (see Refs. [1–3], and references therein). Here we consider scattering from excited states, including long-lived states and hollow-atom states which may be of practical interest [4–6]. Carbon ($Z=6$) was chosen as the scatterer for this exploratory study, since it constitutes a many-electron system without that there are too many electrons to consider. Elastic scattering above and below the *K* edge (but above the *L* edge) is investigated with the hope of using this regime to understand the general scattering situation. Our discussion of scattering from excited states of carbon uses an independent-particle approximation (IPA), and involves an averaging over magnetic substates at the level of the amplitude, exact within the IPA only for fully filled subshells, but in fact generally appropriate within the IPA for the cases considered, which simplifies the discussion and explains most of the general features. However, we also present results for scattering from a hollow lithium atom with and without this approximation in averaging, to illustrate the differences that arise in the case of partially filled subshells (which are generally more prominent when there are fewer electrons present).

The scattering of light is a standard diagnostic technique used to determine particle concentrations and temperatures in plasmas [7,8]. Elastic scattering from bound electrons of excited atoms in the plasma can become important when a laser wavelength is close to a spectral line, as has been shown for the case of hydrogen [9–11], and also for helium [12]. Exact analytic results have been given for Rayleigh scattering of photons from excited hydrogen atoms in the $n=2$ [13] and 3 [14] states, following the corresponding results for ground-state hydrogen [15]. Although there have been some studies of Rayleigh scattering of photons by ions of low nuclear charge [16], the corresponding case involving excited states has received less attention. Ionushauskas *et al*. [17] and Kuplyauskis and Kuplyauskene [18] calculated Rayleigh scattering cross sections in the form-factor approximation for excited zinc and iron atoms and ions at relatively high photon energies compared to the *K*-shell binding energies. Only excitations involving valence electrons were considered.

*Present address: Scientific Computing and Communications Department, Lawrence Livermore National Laboratory, Livermore, CA 94551-0808.

They found the cross sections for scattering to be smaller for excited zinc atoms than for ground-state zinc atoms. As will also be seen here for the case of carbon, they found that finite-angle cross sections for scattering from atoms and ions can coincide at high enough energy. We note the work on photoionization cross sections of excited atoms and ions [19–26], since due to the optical theorem the absorptive part of the forward-angle Rayleigh amplitude can be expressed in terms of the total photoeffect cross section (and the dispersive part may be obtained from it through a dispersion relation). We also note a recent laser spectroscopic study of the high-n Rydberg states of atomic carbon [27].

In our discussion of scattering from excited states of carbon, we employ the S-matrix approach previously used to describe elastic scattering from ground-state atoms in the IPA [28,1]. This approach performs an averaging over the magnetic substates of a subshell at the level of the scattering amplitude, with the result being weighted according to the number of electrons present in that subshell. This is exact within the IPA only for fully filled subshells. Nevertheless it is generally a good approximation of the properly-averaged IPA result for scattering from ground-state atoms, since most electrons are in fully filled subshells, and it accounts for the dominant components of the coherent scattering [29,30]. (A noticeable exception is the existence of near-zeros in the cross section above resonances in the averaged-amplitude approach for hollow-atom configurations. These near-zeros can be spurious, as will be seen in the more proper treatment discussed in Sec. VI.) Below we consider the consequences of IPA assumptions in scattering.

The observables of elastic scattering are the momentum and polarization $(\hbar \boldsymbol{k}_i, \boldsymbol{\epsilon}_i)$ and $(\hbar \boldsymbol{k}_f, \boldsymbol{\epsilon}_f)$ of the incident and scattered photons and the state of the atom, which is unchanged by the process (due to the averaging over magnetic substates mentioned earlier—this neglects elastic incoherent scattering, which will be addressed in Sec. VI). The total elastic amplitude is obtained by summing Rayleigh, Delbrück, and nuclear amplitudes, though it is expected that the Rayleigh amplitude, describing elastic scattering off bound electrons, is dominant in the energy range considered here.

In this work various excited atomic state configurations are chosen so as to see the effects of both core excitations (meaning that a vacancy is present in the innermost orbitals) and outer-electron excitations, leaving the innermost orbitals undisturbed. Hollow atoms are considered in which the K shell is completely vacant, with the electrons placed in higher shells in various configurations. There has been much recent interest in the observation and classification of such hollow atomic states (resonances) for the case of lithium [31,6].

Electron orbitals are obtained in a relativistic screened self-consistent Dirac-Slater-type central potential. The Rayleigh scattering amplitude A^R is obtained, in the IPA, by calculating, in partial waves and multipoles, the second-order S-matrix element in the central potential, summing over separate amplitudes A_n^R for scattering off each bound electron in the potential. This method, developed by Brown *et al.* [32], Johnson and Feiock [33], and Kissel and co-workers [28,1], was used previously to investigate scattering from ground-state neutral atoms and ions [34,35]. The calculation is fully relativistic, and it has been used to describe scattering from high-Z atoms such as uranium, where a relativistic description is necessary.

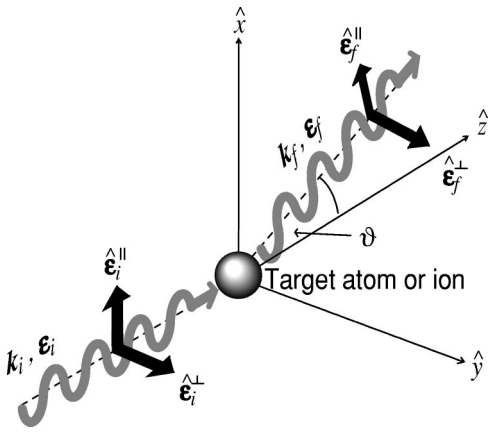

FIG. 1. Coordinate system used. The incident photon is scattering though an angle θ. The photon polarization vectors can be resolved into components parallel and perpendicular to the scattering plane.

We use a local-exchange model of the atom, and therefore neglect nonlocal-exchange effects (as in the Hartree-Fock method) and electron correlations (beyond the Hartree-Fock method). Correlation effects are expected to be important in resonance regions, though the dominant effect is the shifting of threshold positions. Nonlocal-exchange effects have been seen to matter at the 10% level well above threshold for neon in a recent experiment [36], though the effect was only this large for a limited range of momentum transfers. In light elements one can anticipate $O(1/Z)$ IPA breaking contributions to p-state anomalous amplitudes even at higher energies, as observed in $2p$ photoionization of neon by Dias *et al.* [37], with larger effects on the (small) d- and f-state anomalous amplitudes [38]. However, at higher energies, form-factor contributions dominate at the forward angles where cross sections are larger.

For carbon, relativistic effects are not important, and we will use a nonrelativistic configuration notation throughout. The configuration of the ground state is taken to be $(1s)^2(2s)^2(2p)^2$. Incident photon energies ranging from 100 eV to 10 keV are considered. This range includes all bound-bound transition energies involving the K shell, and excludes all other bound-bound transition energies, which are below 100 eV. By looking at this region, one obtains a picture of what happens in the neighborhood of a resonance without the degree of complication that exists at lower energies. (Behavior in the vicinity of the lowest atomic resonances can be understood by looking at the analytic results for hydrogen in ground or excited states [13–15].) By 10 keV one is well above all resonances and edges, allowing the process in this low-Z case to be well described in terms of the relatively simple form-factor approach.

The coordinate system we use is shown in Fig. 1. Resolving the polarization vectors of the incident and scattered photon into components parallel and perpendicular to the scattering plane,

$$\boldsymbol{\epsilon}=\epsilon^{\parallel}\hat{\boldsymbol{\epsilon}}^{\parallel}+\epsilon^{\perp}\hat{\boldsymbol{\epsilon}}^{\perp}, \tag{1}$$

magnetic substate averaging at the level of the scattering amplitude permits one to write the scattering amplitude as

$$A^R=\epsilon_i^{\parallel}\epsilon_f^{\parallel}*A_{\parallel}+\epsilon_i^{\perp}\epsilon_f^{\perp}*A_{\perp}, \tag{2}$$

where $A_{\parallel}(\omega,\theta)$ and $A_{\perp}(\omega,\theta)$ are invariant amplitudes depending on the photon energy ω and the scattering angle θ. It is seen from Eq. (2) that if the photon polarization is initially parallel or perpendicular to the scattering plane, it will remain so after scattering. The unpolarized differential cross section (unpolarized incident photon beam, scattered photon polarization not measured), obtained by summing over the scattered photon polarizations and averaging over the initial photon polarizations, is

$$\frac{d\sigma}{d\Omega}=\frac{1}{2}(|A_{\parallel}|^2+|A_{\perp}|^2). \tag{3}$$

In the forward direction the parallel and perpendicular amplitudes are equal:

$$A_{\parallel}(\omega,0)=A_{\perp}(\omega,0)\equiv A(\omega,0). \tag{4}$$

The Thomson amplitudes for scattering from a free electron (corresponding to the classical result for scattering from a point charge) are

$$\mathrm{Re}\,A_{\perp}^T=-r_0, \quad \mathrm{Re}\,A_{\parallel}^T=-r_0\cos\theta, \tag{5}$$

where r_0 is the classical electron radius, and the imaginary parts vanish. From Eq. (3) we see that this leads to a cross section with a $(1+\cos^2\theta)$ angular dependence. For scattering from an atom one should sum the amplitudes over all the electrons present, which in this free-electron approximation simply means multiplying the amplitudes in Eq. (5) by the number N of electrons in the atom.

A better, yet still simple, way to approximate the Rayleigh amplitude for an atom utilizes the form factors [39] for the nth electron and for the atom:

$$f_n(q)=4\pi\int_0^{+\infty}\rho_n(r)\frac{\sin(qr)}{qr}r^2dr, \quad f(q)=\sum_n f_n(q), \tag{6}$$

where $\hbar q$ is the momentum transfer to the atom in scattering, and $\rho_n(r)$ is the charge density of the nth electron; $f_n(0)=1$ and $f(0)=N$ is the number of electrons in the atom. In this form-factor (FF) approximation,

$$\mathrm{Re}\,A_{\perp}=-r_0f(q), \quad \mathrm{Re}\,A_{\parallel}=-r_0f(q)\cos\theta, \tag{7}$$

and the imaginary parts of the amplitude vanish. The forward cross section is constant, independent of the energy. In the dipole approximation (corresponding nonrelativistically to replacing $e^{i\mathbf{k}\cdot\mathbf{r}}$ by 1 in the expression for the photon operators) the form factor is replaced by its forward-angle value at all scattering angles, leading back to the Thomson cross section with its $(1+\cos^2\theta)$ angular dependence. The contribution of higher multipoles suppresses the cross section at more backward angles relative to the forward angle, such that the angular distribution becomes increasingly forward peaked at high energy. Higher multipoles typically become important for a given subshell when the momentum transfer is comparable with the average momentum of the bound electron(s) in that subshell. Of course in calculating the form factor directly as in Eq. (6) there is no need to perform a multipole expansion (all multipoles are included). For a discussion of higher-order multipoles and retardation in Rayleigh scattering, see Ref. [40].

The form-factor approximation fails for a given subshell when the photon energy is comparable to or below the binding energy of the subshell, or close to the energy of a bound-bound transition, or for high Z at high energy and large scattering angle [41]. The FF approximation may be used in the low-Z cases being considered here to calculate the subshell Rayleigh amplitudes when the photon energy is much greater than the binding energy of the subshell.

In the nonrelativistic approximation, $\mathrm{Re}\,A(\infty,0)=-f(0)r_0=-Nr_0$, where N is the number of bound electrons. The anomalous scattering factors f' and f'' are defined as the difference (taking out the factor $-r_0$) between the full forward amplitude at finite energy and the high-energy limit:

$$A(\omega,0)=-r_0[f(0)+f'(\omega)+if''(\omega)]. \tag{8}$$

The anomalous scattering factors f' and f'' defined in this way give the difference between the full forward scattering amplitude, characterized by $f(0)+f'+if''$, and the result $f(0)$ within the form-factor approximation at forward angle. At x-ray energies and below it is a fairly good approximation to extend this approach to finite angle by assuming angle-independent anomalous scattering factors (as would be obtained in dipole approximation), writing the amplitudes as in Eq. (7), but with $f(q)$ replaced by $f(q)+f'+if''$, giving a form-factor plus angle-independent anomalous scattering factor (FF + ASF) approximation for the cross sections. The success of this approach is due to the fact that higher-multipole effects in the ASF are generally less important than higher-multipole effects in the FF at the same energy [40]. One is neglecting higher multipoles in the ASF but including the full angle dependence of the FF (i.e., including all FF multipoles). (One can also go beyond this to consider the full angular dependence of the anomalous scattering factors, given by the inclusion of the higher multipoles, which also requires including further anomalous scattering factors that vanish at forward and backward angles [42].) Note that in the S-matrix approach one is calculating all significant multipoles, considering the full angle dependence of both the (IPA) FF and ASF contributions. A discussion of the general validity of the FF and (FF + ASF) approximations was given in Ref. [41]. As already noted, there is a connection between the total photoeffect cross section σ^{PE} and the anomalous Rayleigh amplitudes f' and f'', with $\mathrm{Im}\,A(\omega,0)=-r_0f''=(\omega/4\pi c)\sigma^{PE}$ in this nonrelativistic case except at the bound-bound transition energies (f' is then related through a dispersion relation [1]).

In Sec. II we give an overview of the predicted behavior of excited-state differential scattering cross sections, for dif-

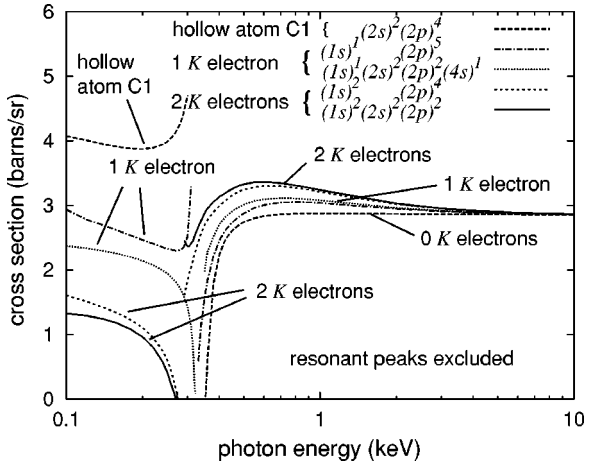

FIG. 2. Forward-angle cross section for the ground-state configuration and various excited-state configurations of carbon. The details of the resonant peaks are omitted. There is a clear separation of cross sections for configurations with different numbers of $1s$ electrons. Cross sections approach a common high-energy limit along one of three curves according to the number of $1s$ electrons.

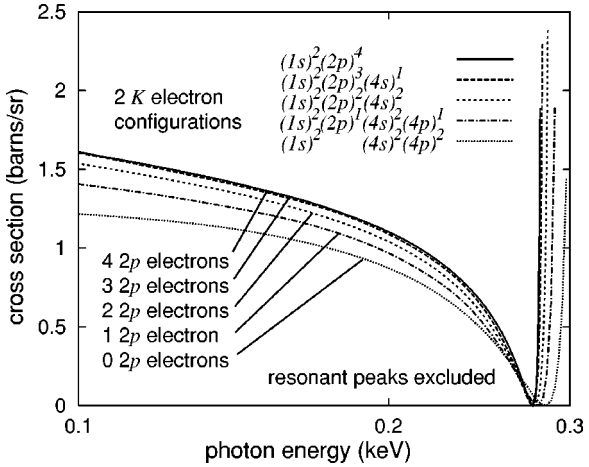

FIG. 3. Forward-angle cross section below the resonance region for configurations of carbon with two $1s$ electrons and different numbers of $2p$ electrons. The details of the resonant peaks are omitted. The cross sections for configurations with three and four $2p$ electrons are similar. All cross sections drop sharply as the $1s \leftrightarrow 2p$ resonance is approached from below.

ferent configurations, as a function of photon energy and scattering angle. Section III describes the individual subshell amplitudes, focusing on forward-angle scattering, in order to understand the way in which amplitudes from different subshells combine to give the scattering cross section for the excited atom or ion. Individual amplitudes have ''spurious'' resonances, due to transitions between occupied subshells, which cancel in the total amplitude. In Sec. IV cross sections at forward angle are explained in terms of the individual subshell amplitudes. It is found that in certain configurations there will be deep minima in the cross sections below the resonance regions, corresponding to a zero in the total real amplitude. Some hollow-atom configurations will have elevated cross sections below the resonance region. Section V discusses the angular dependence of cross sections and the behavior of the total integrated cross sections. The extent to which the angular dependence of cross sections can be understood in terms of angle-dependent form factors and the angle-independent anomalous scattering factors is discussed. We show that ions and neutral atoms have similar cross sections at high energy and finite angle, if the configurations of the core electrons are the same. Total integrated cross sections for hollow-atom states are compared with the corresponding ground-state cross section. In Sec. VI we consider the consequences of the approximation of averaging over magnetic substates at the level of the scattering amplitude. We use scattering from a hollow-lithium-atom configuration to illustrate the differences which arise when a more correct procedure is utilized. Conclusions are presented in Sec. VII.

II. GENERAL FEATURES

In this section we present an overview of the features of excited-state differential and total cross sections, seen in Figs. 2–8, which in this light element are approaching form-factor predictions at high energies for all angles. (For high Z anomalous amplitudes would remain important at large angles at high energy.) In Sec. III the form of the subshell amplitudes is discussed, which in subsequent sections allows us to give detailed explanations for the features highlighted here. Carbon has been chosen as it is a many-electron atom, illustrating the general many-electron situation, but it does not have too many electrons which would complicate the discussion.

For convenience we classify and label the hollow atom

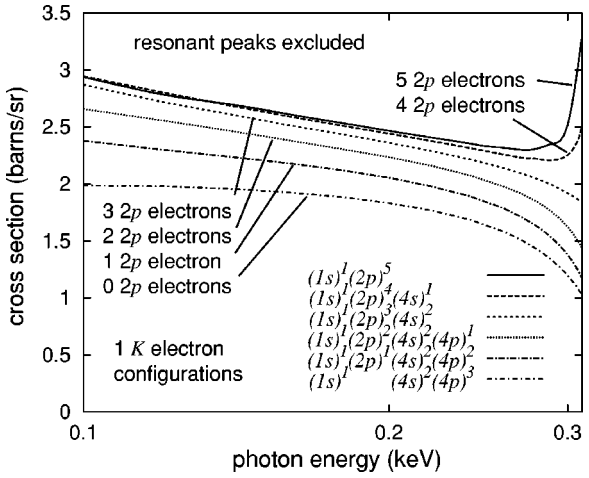

FIG. 4. Forward-angle cross section below the resonance region for configurations of carbon with one $1s$ electron and different numbers of $2p$ electrons. The details of the resonant peaks are omitted. The cross sections for configurations with four and five $2p$ electrons are similar, and do not drop sharply as the resonance region is approached from below as there are a net number of downward $L \rightarrow K$ transitions. Configurations with a half-filled or less than half-filled $2p$ shell have cross sections that begin to drop sharply as the resonance is approached from below; however, the features just below the resonance can be washed out by additional effects beyond the averaged-amplitude approximation used here, and so are not shown.

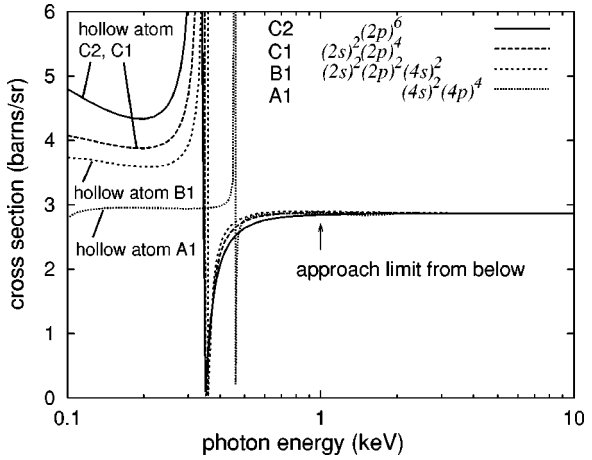

FIG. 5. Forward-angle cross section for hollow-carbon-atom configurations. The cross section for the case with all the electrons present in the *N* shell is close to the form-factor values both above and below the resonance region, through it starts to deviate at low energy as the region of downward transitions to the *L* shell is approached. Configurations with all the electrons present in the *L* shell have elevated cross sections below the resonance region because of the strong $2p \rightarrow 1s$ downward transition and the imaginary components of the *L*-shell amplitudes, which become significant close to 100 eV. The cross sections quickly coincide above the resonance region, approaching the high-energy limit from below.

and ion configurations considered. All hollow atom or hollow ion states considered have a vacant *K* shell, with electrons being placed in the *L* shell or *N* shell or both:

label	configuration	description
A1	$(4s)^2(4p)^4$	hollow atom, electrons in *N* shell.
B1	$(2s)^2(2p)^2(4s)^2$	hollow atom, electrons in *L*, *N* shells.
C1	$(2s)^2(2p)^4$	hollow atom, electrons in *L* shell.
C2	$(2p)^6$	hollow atom, electrons in *L* shell.
C3	$(2s)^2(2p)^2$	hollow ion, electrons in *L* shell.

We will subsequently refer to specific hollow atom and hollow ion configurations using the labels defined above.

Figure 2 shows the forward-angle differential cross section as a function of energy for a variety of configurations with differing numbers of $1s$ electrons. The energy range (photon energies ranging from 100 eV to 10 keV) includes the *K* edge for all cases but does not include any of the *L* edges, though 100 eV is not far from the highest *L* edges. The binding energy of the *K* shell is greater for excited states than for the ground state. This effect is most prominent for core excitations where $1s$ electrons are excited. The removal of core electrons makes the atom less screened and more Coulombic, so that binding energies and binding-energy differences increase. Note that all cross sections converge at high energy toward the expected form-factor value of 2.86 b/sr, which depends only on the number of electrons and is the same for all configurations of the same ionicity. Cross sections for configurations with the same number (0, 1, or 2) of $1s$ electrons approach the form-factor value along a common curve, giving rise to the three distinct curves. Below the

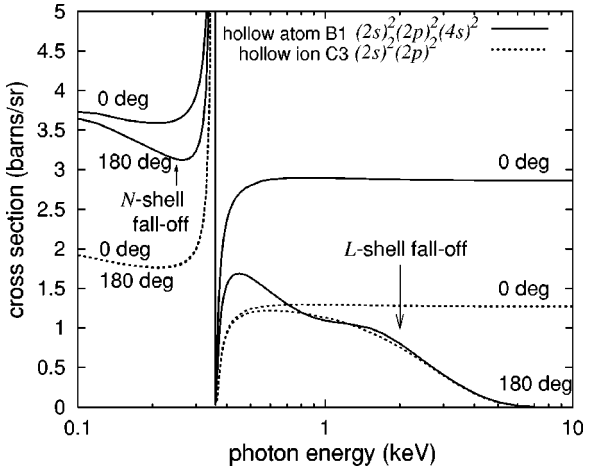

FIG. 6. Forward and backward scattering cross sections for a hollow neutral carbon atom and a hollow carbon ion. The configuration of the hollow atom differs from that of the hollow ion only in that it has two more electrons in the $4s$ state. The cross sections are seen to coincide at backward angle at high energy. Below the resonant region, cross sections are similar at forward and backward angles within a given configuration, and are clearly different for the atomic and ionic cases.

K-shell threshold interference effects between the *K*-shell amplitudes and the *L*-shell amplitudes, dependent on the occupation of the shells, cause very different behaviors of the cross section for different configurations. We will return to these features in Sec. IV on forward scattering.

In Figs. 3 and 4 forward-angle cross sections below the resonance region are shown in more detail for configurations

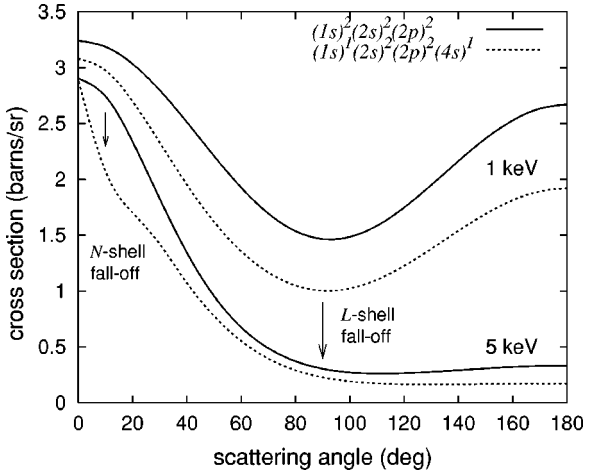

FIG. 7. Angular dependence of the cross section at fixed energies for the ground-state configuration of carbon and a carbon configuration with one $1s$ electron excited to the $4s$ state. At 1 keV the anomalous pieces of the *K*-shell amplitudes are still significant, resulting in different values for the cross section at forward angle. The angular distributions are still close to the simple dipole form valid at low energies. At 5 keV the anomalous pieces are not important, hence the cross sections agree at forward angle. The $4s$ amplitude falls off much faster with increasing angle at this energy, resulting in a sharp drop in the excited-state cross section at small angles.

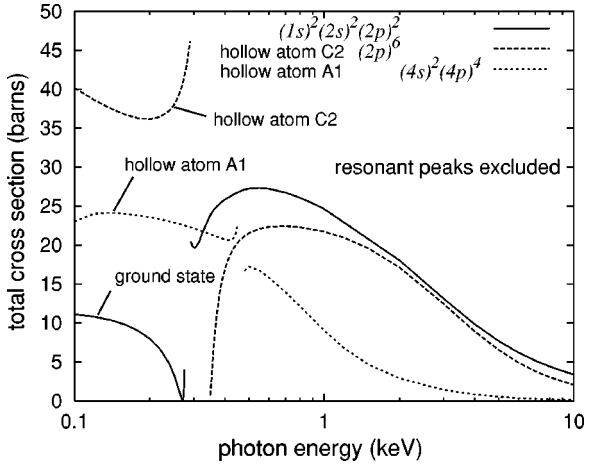

FIG. 8. Total cross section (integrated over angles) as a function of energy for the ground-state and hollow-carbon-atom configurations. The ground-state cross section is small below the resonance region, as the $1s$ electrons are not contributing. The hollow atom with all the electrons present in the L shell has the largest cross section below the resonance region. Above the resonance region, as the energy is increased, the cross section for the hollow atom with all the electrons present in the N shell drops most rapidly as the scattering from it becomes more forward peaked. The ground-state cross section and that for the hollow atom with all the electrons present in the L shell fall off at nearly the same rate since they both involve many L-shell electrons. The ground-state cross section is greater at high energies due to scattering off the tightly bound $1s$ electrons, whose angular scattering profile is less forward peaked than those of higher-shell electrons.

that involve two $1s$ electrons and one $1s$ electron, respectively. Configurations are exhibited that have different numbers of electrons in the $2p$ state, with any remaining electrons being placed in the N shell, and the configurations therefore have different numbers of net upward or downward $1s \leftrightarrow 2p$ transitions. Given that the $1s \leftrightarrow 2p$ transitions are the strongest involving the K shell, there are striking differences among the cross sections for these configurations. In Fig. 3 (the fully filled K shell) the cross section is higher for configurations with more $2p$ electrons, though the difference for configurations involving four and five $2p$ electrons is slight. For all configurations there is a sharp drop in the cross section as the resonance region is approached from below (which is partially filled in when one goes beyond the averaged-amplitude approach). Figure 4 (the half-filled K shell) shows similar qualitative properties far enough below the resonance. The configurations with four or five $2p$ electrons do not differ much from each other away from the resonance region. The linear behavior of the cross sections at low energy persists to higher energies relative to the resonance position than is the case in Fig. 3. Further discussion is given in Sec. IV. The behavior just below the resonance region (where the averaged-amplitude approach predicts sharp drops in the cross sections for the configurations with zero, one, two, and three $2p$ electrons) is not shown in detail as it is adversely affected by effects beyond the averaged-amplitude approach, as will be discussed in Sec. VI.

Figure 5 shows the differential cross section at forward angle for scattering from four different hollow-atom configurations. These cross sections approach the form-factor value at high energies from below, in contrast to the situation for configurations with a fully filled or partially filled K shell (see Figs. 2–4). Below the resonance region the cross sections for configurations involving L-shell electrons are noticeably larger than the form-factor value. The cross section for the hollow atom A1 is close to the form-factor value throughout the region, except near its (narrow) resonance, and also at low energies, where the region of downward transitions to the L shell is being approached. One can see that the position of resonances corresponding to downward transitions to the empty K shell shifts toward higher energies as the atom becomes more hollow, while the width of the resonances narrows, corresponding to transitions from more outer shells to the K shell. The hollow atoms C1 and C2 have cross sections below the resonance region that are considerably larger than the form-factor value. For further discussion, see Sec. IV.

Figure 6 shows the energy dependence of the differential cross section at backward and at forward angle for the hollow neutral atom B1 and for the hollow ion C3 of ionicity $+2$. The hollow atom B1 differs from the hollow ion C3 only in that it has two more electrons, placed in the $4s$ state. Above the resonance region the cross sections behave quite differently at forward angle. Well above the K edge both configurations have constant forward cross sections, corresponding to different numbers N of electrons in the two configurations. The cross sections at backward angle for the two configurations are seen to quickly converge with increasing energy. Below the resonance region the cross sections at forward and backward angle are similar within a given configuration, and the cross sections are clearly different for the atom and the ion, which will be explained in Sec. V.

We now look further at the behavior of the cross section as a function of angle, before considering the total integrated cross sections (integrated over all angles). Figure 7 shows the scattering cross section as a function of angle at 1 and 5 keV for the ground state and an excited state with configuration $(1s)^1(2s)^2(2p)^2(4s)^1$. At 1 keV the cross section for the ground state has an angular dependence close to the $\propto(1+\cos^2\theta)$ behavior expected in a dipole-dominant regime, and this is true to a lesser extent for the excited case. At 5 keV the cross section for the excited case is seen to fall rapidly at first, corresponding to falloff of the subshell amplitude for the electron in the $4s$ state. The cross section is lower for the excited state than for the ground state at larger angle because there is effectively one less electron to scatter from. For further details, see Sec. V.

Figure 8 compares the total integrated cross sections for hollow atoms (which have electrons placed in the L or N shell) with that for the ground-state configuration, as a function of energy. The ground-state cross section is small below the resonance region, as the K electrons are not contributing. The hollow atom C2 has the largest cross section below the resonance region. Above the resonance region, as energy is increased, the cross section for the hollow atom A1 drops most rapidly, as the scattering from it becomes more forward peaked. The ground-state and the hollow-atom C2 cross sec-

tions fall off at nearly the same rate above the resonance region, though the ground-state cross section remains larger than the hollow-atom C2 cross section. For further details, see Sec. V. In the next sections we shall try to understand the origins of these observed features.

III. INDIVIDUAL SUBSHELL AMPLITUDES

Figure 9 gives a schematic description of the averaged real $-(1+f')$ and imaginary $-(f'')$ forward amplitudes (per electron in units of r_0) for the K, L, and M shells, neglecting a detailed dependence on the choice of subshell. These amplitudes correspond to averaging over magnetic substates for a given subshell at the level of the scattering amplitude (the averaged-amplitude approach). We begin by summarizing the main features which are illustrated in the figure. (1) For each subshell, as one increases the energy from $\omega=0$, there is a gradual ($\propto\omega^2$) rise of the real amplitude to a region of a Rydberg series of upward transitions, i.e., $f'(0)=-1$ and is becoming more negative, causing the real amplitude $-(1+f')$ to become more positive. (2) Going across the threshold, the eventual outcome is a finite negative step in the real amplitude to $\leqslant -1$, i.e., $f'\geqslant 0$. (3) Amplitudes are finite at threshold (approached from above): f'' turns on at threshold (being large in magnitude there), falling off with increasing energy, faster than f'. (4) Above the threshold for a given subshell, there are subsequent isolated resonant downward transitions corresponding to δ functions in f'' affecting f' in regions near each downward transition, with a finite positive step in the amplitude (except for the K shell, for which there are no downward transitions, as it is the most deeply bound shell). The largest of these steps is that in the L-shell amplitude associated with the $L\rightarrow K$ transition, as is indicated. (5) The sum of all steps in an amplitude f' is 1, so $f'(\infty)=0$, and the real amplitude is equal to -1 in the high-energy limit. (6) Resonances corresponding to transitions between fully filled subshells in a given configuration are spurious; they cancel in the sum of amplitudes corresponding to that configuration.

In the independent-particle approximation, the whole-atom Rayleigh scattering amplitude A^R is the algebraic sum of the individual electron amplitudes A_n^R. Since the amplitude for scattering off a particular bound electron is calculated independently of the occupation of all other bound states, all single-photon bound-bound transitions are included in the summation. The scattering amplitude, for the nth electron, is [1,2]

$$A_n^R = r_0 mc^2 \sum_p^{\mathcal{F}} \times\left[\frac{\langle n|\mathcal{A}^*|p\rangle\langle p|\mathcal{A}|n\rangle}{E_n-E_p+\hbar\omega}+\frac{\langle n|\mathcal{A}|p\rangle\langle p|\mathcal{A}^*|n\rangle}{E_n-E_p-\hbar\omega}\right], \quad (9)$$

where p is a sum over all intermediate single-particle states, regardless of occupation, and $\mathcal{A}$ ($\mathcal{A}^*$) is the absorption (emission) electron-photon interaction operator. The total amplitude A^R is obtained by summing n over all electrons. The amplitude A_n^R will show a resonance structure whenever the photon energy corresponds to a bound-bound transition energy, for transitions between the bound state $|n\rangle$ and an intermediate bound state $|p\rangle$. If, however, the single-particle bound state $|p\rangle$ is occupied, such a resonance is unphysical. In summing over all occupied, orbitals to obtain the total amplitude, there will be an exactly canceling resonant term in the amplitude A_p^R corresponding to transitions from the

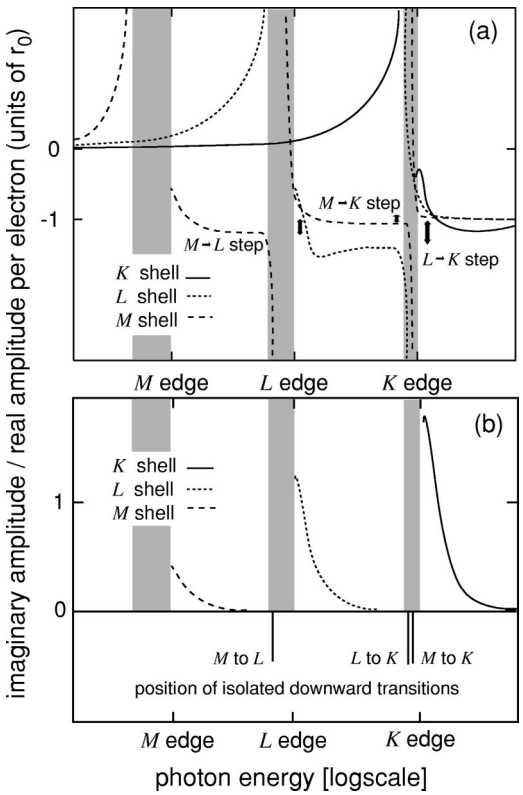

FIG. 9. (a) Schematic illustration of the K-, L-, and M-shell real amplitudes (per electron) at forward angle. The amplitudes have a common negative limit at high energy. As the energy is decreased the amplitudes pass through a series of isolated resonances corresponding to downward transitions (with the exception of the K shell) to more tightly bound shells. Associated with each downward transition is a step in the amplitude, related to the bound-bound transition strength, with the amplitude being more negative below the resonance. The largest step is in the L amplitude, associated with the strong $L\rightarrow K$ transition, followed by those in the M amplitude associated with the $M\rightarrow L$ and the $M\rightarrow K$ transitions. The amplitudes approach a finite value as the edge for that shell is reached. Below the edge there is a Rydberg series of resonances corresponding to upward transitions, represented by dark bands. Below the lowest-lying resonance the amplitude approaches zero from above, proportional to ω^2 at low energy. (b) The corresponding imaginary parts rise to a finite value as the edges are approached from above. The amplitudes also contain δ-function terms whenever the energy equals that of a bound-bound transition. Below the edge for a given shell, the amplitude for that shell vanishes, except for the Rydberg series δ-function terms just below the edge corresponding to upward transitions to higher shells, represented by dark bands. The location of the isolated downward transitions are indicated. The imaginary amplitudes are always positive, except for negative δ-function terms at energies corresponding to downward bound-bound transitions.

occupied bound state $|p\rangle$ to the occupied bound state $|n\rangle$. Consequently all subshell amplitudes (corresponding to subshells that are partially or fully occupied) will contain resonant terms corresponding to transitions to all other subshells (though these resonances may be very weak, as in the case of dipole-forbidden resonances). In the total amplitude, however, there will not be resonant terms corresponding to transitions between subshells that are both fully filled, or are both half-filled, as the resonant terms for each subshell amplitude cancel exactly in the averaged-amplitude approach. (There also will not be resonances corresponding to transitions between subshells that are both unoccupied.) More generally, upward and downward resonances cancel if the number of upward and downward transitions are equal, i.e., if the number of electrons n_A and n_B in subshells A and B containing N_A and N_B substates, respectively, satisfy $n_A N_B = n_B N_A$, for example $(p)^1(g)^3$. (See Sec. VI for a discussion of the extent to which this cancellation of resonances depends on the averaged-amplitude approximation.)

We note that the averaged-amplitude approach is exact within the IPA for fully filled subshells, and it is approximate for partially filled subshells. This approximation in particular neglects elastic incoherent scattering, present when there are partially filled subshells. In the more proper treatment (involving an averaging over cross sections for all possible magnetic substate configurations) there will be additional amplitudes. Nevertheless the magnetic substate averaging approximation generally works well for scattering from many-electron atoms, since it takes account of the dominant coherent scattering; this allows us to discuss the general features of scattering from excited states using the schematic amplitudes of Fig. 9. We shall revisit this issue in Sec. VI.

Figure 9 is only intended to give a picture of the general form of the amplitudes, as there are details that will be particular to a specific configuration. If we look at the subshell amplitudes, in the case of the K shell resonances will appear just below the K edge, corresponding to transitions to all the higher shells, some of which will be (partially) filled. For L-shell amplitudes, resonances will appear in two different regions. One region, with a behavior similar to that for the K shell, will be below the L edge, and the resonances are similar to those for K shell, though now corresponding to transitions to all shells above the L shell. Since the L edge for carbon states is generally of the order of tens of eV, this feature does not fall within the energy range studied. The second resonance region of the L-shell amplitudes corresponds to the energy of downward bound-bound transitions from the L shell to the K shell. This feature will appear even for configurations where the K shell is filled, such as the ground state, since the calculation of a subshell amplitude includes transitions to all other states.

A common description applies to all (partially) filled shells. As is seen in Fig. 9, all given real forward amplitudes for scattering from a bound electron have a common negative high-energy limit. As the energy is decreased an amplitude passes through a set of widely spaced resonances corresponding to downward transitions to lower-lying shells. Except for these resonances the amplitude remains negative, becoming more negative below each resonance. The amplitude approaches a finite value as the edge for the shell in question is reached. Just below the edge there is an infinite sequence of resonances corresponding to the Rydberg series of upward transitions to higher shells. As the energy is further decreased the amplitude approaches zero from above, proportional to ω^2 at low energy.

The imaginary amplitudes rise to a finite value as the edges are approached from above, as for the photoeffect total cross section, which is related to the imaginary amplitude through the optical theorem. The imaginary amplitudes also contain positive (negative) δ-function terms whenever the energy is equal to that of an upward (downward) bound-bound transition. Below the edge for a given shell the imaginary amplitude for that shell vanishes, except for the infinite sequence of positive δ-function terms just below the edge corresponding to upward transitions to higher shells. The L- and M-shell imaginary amplitudes contain a negative δ-function term corresponding to downward transitions to the K shell, the M-shell imaginary amplitude also containing such a term corresponding to downward transitions to the L shell. The imaginary amplitudes are always positive, except for δ-function terms at energies corresponding to downward bound-bound transitions.

For a given subshell amplitude, there are small differences for different configurations, primarily shifts in the positions of the edges and the bound-bound transition energies and changes in the bound-bound transition strengths. (There can also be shape and structure effect changes near threshold, as in the corresponding photoeffect cross sections.) The total amplitude for scattering will depend on which subshells the electrons are placed in, i.e., the choice of configuration, primarily in determining what subshell amplitudes are to be summed, and with what weights.

The previous discussion has been for the forward scattering subshell amplitudes. The subshell amplitudes at finite angle can be well approximated by the angle-dependent form factor and the anomalous scattering amplitudes (taken to be angle independent), as defined for that subshell. The K-shell amplitude has a dipole behavior for the energy range considered. The L-shell amplitude has a dipole behavior below the resonance region, and it falls off above the resonance, though there is still a contribution to backward-angle scattering at 10 keV. The N-shell amplitude has a dipole behavior at 100 eV, but it immediately begins to fall off through the K resonance region. In the next sections the features in the scattering cross sections which were identified in Sec. II will be explained in terms of the behavior of the subshell amplitudes, considering the regions above and below the K edge, but above the L edge.

IV. FORWARD-ANGLE SCATTERING

It was seen in Fig. 2 that the forward-angle cross sections for different configurations approach the high-energy limit along one of three common curves depending on the number of $1s$ electrons in the configuration. For hollow atoms with no $1s$ electrons the high-energy limit is approached from below. For configurations with one or two $1s$ electrons there is a maximum in the cross section above the K edge, and the

high-energy limit is approached from above. (Note that this is not the case for high-Z atoms.) This behavior can be understood from the form of the K-shell amplitude seen in Fig. 9. As one moves away from the K edge toward the high-energy limit, the real part becomes slightly more negative than the form-factor value (this detail is particular to low-Z atoms), the difference being given by f'. As we are above all edges in this region, all real subshell amplitudes are negative, and will sum without cancellation; the L- and higher-shell amplitudes approach FF values while the K-shell amplitude is still changing. The imaginary parts are important just above threshold, but their contribution to the cross section quickly falls off with increasing energy. The minimum in the real part of the K-shell amplitude (and to some extent the large-near-threshold imaginary amplitude) gives rise to a maximum in the cross section. The imaginary part falls off quickly, so that the form of the curves as the high-energy limit is approached is governed by f' alone. The K-shell real and imaginary amplitudes for configurations with the same number of $1s$ electrons coincide well above the K edge, giving rise to the common curves.

In Fig. 3, for configurations with two electrons in the $1s$ state, all cross sections exhibit a deep dip as the resonance region is approached from below. Since the K shell is fully filled, any physical transition between the K shell and any other shell must be an upward transition. If that other shell is also fully filled then there can be no physical transition between the two. Looking now at the K-, L-, and M-shell amplitudes shown in Fig. 9, one first sees that the general features just below the resonance region are going to be dominated by the real amplitude, since the K-shell imaginary component vanishes below the resonance region and the higher-shell imaginary component is relatively small. Well below the resonance region, the net real amplitude will be negative, since the positive K-shell amplitude is becoming small and the real amplitudes for the other shells are negative. As the resonance region is approached from below, the positive K-shell real amplitude becomes large, corresponding to upward transitions to all other shells, while the higher-shell real amplitude becomes large and negative, corresponding to downward transitions to the K shell. Summing up, to obtain the total real amplitude, upward and downward resonant contributions corresponding to transitions between occupied states should cancel. Since the physical transitions must be upward, the net real amplitude must be positive just below the resonance region, i.e., as one becomes close to the K-shell resonance region from below, the surviving resonances are upward resonances of the positive K-shell amplitude, so that as the first resonance is approached from below the positive K amplitude grows. Thus the total real amplitude must change sign; there is a zero in the real amplitude below the resonance region, and all configurations involving a fully filled K shell are expected to exhibit a deep dip in the cross section at an energy corresponding to the zero in the real amplitude.

The near-zero observed in the cross sections is seen to occur at a lower energy for configurations with more $2p$ electrons. This is primarily due to the downward shift of the K-shell binding energies, and the resulting decrease in the energies of the upward transitions from the K shell, for configurations with more electrons in the L shell rather than in outer shells (more L electrons increases the screening of the K shell). However, this downward shift of the near-zeros due to the shift in the binding energy is partially compensated for by a shift upward, since with more $2p$ electrons the negative higher-shell real amplitude is larger and cancels the positive K-shell real resonant amplitude closer to the first real resonance. We note that effects beyond the averaged-amplitude approach (including incoherent elastic scattering and unresolved inelastic contributions, as described in Sec. VI) tend to partially fill in the near-zeros. These additional contributions are large close to resonance, quickly becoming small away from resonance, such that the near-zeros seen in the configurations with two K electrons are still apparent.

We note the separation of cross sections with different numbers of $2p$ electrons below the resonance region. From Fig. 9 it is seen that there is a noticeable step in the per-electron L-shell real amplitudes in passing through the downward resonance to the K shell, related to the strength of the $2p \leftrightarrow 1s$ resonance, with the amplitude being more negative below the resonance. Therefore configurations with more $2p$ electrons (rather than putting them in the N shell, where they would give a FF contribution) have greater cross sections, due to this step. However when one has many L-shell electrons, screening effects begin to decrease the resonance strength, hence also decrease the size of the per-electron step. As a result there is no clear separation of cross sections with three and four $2p$ electrons (i.e., increasing the number of electrons from three to four is compensated for by the decrease in the size of the per-electron step). Therefore one is increasing the cross section as one increases the number of $2p$ electrons from zero, but as the subshell becomes close to being fully filled the screening effects become dominant and there is no longer any substantial increase in the cross section as the number of $2p$ electrons is increased.

The situation is more complicated for configurations with one electron in the $1s$ state, as shown in Fig. 4. Now there is the possibility of having a net downward number of transitions to the K shell from other shells. Within the averaged-amplitude approximation this implies that configurations with zero, one, two, or three electrons in the $2p$ state still exhibit a deep dip in the cross section as the resonance region is approached from below, as in Fig. 3. For zero, one, or two $2p$ electrons the $2p$ shell is less than half filled and the net number of transitions is upward, so the previous argument given for the case of a fully filled K shell still applies. For the configuration with three $2p$ electrons the net number of transitions is zero, meaning the $1s \leftrightarrow 2p$ resonant contributions cancel in the averaged-amplitude approach. However, the averaged-amplitude approach would still predict a deep dip, since the same argument applies to transitions between the $1s$ and $3p$ states, the next strongest resonance (and the M shell is vacant for all configurations shown). In this case the near-zero in the cross section is at a higher energy since the resonance being approached is at a higher energy. [In fact for any excited carbon configuration of the form $(1s)^1(2p)^3 \ldots$ this will be the case, as there are not enough remaining electrons to more than half fill the $M_{2,3}$ subshell,

giving a net upward number of transitions.] However with only one electron in the K shell the positions of the averaged-amplitude near-zeros occur closer to resonance, where effects beyond the averaged-amplitude approach are large, and tend to fill in the near-zeros. Therefore, we do not show this detail just below resonance.

Once there are more than three electrons in the $2p$ state there is a net downward number of transitions. So in the total real amplitude there is no zero before the large negative $L_{2,3}$-subshell downward resonant amplitude begins to dominate. Therefore, even the averaged-amplitude approach predicts no sharp dip for these cases. There still is a slight dip in the cross section due to the gradually increasing positive K-shell real amplitude (before the real negative net $2p \rightarrow 1s$ narrower downward resonant transitions dominate), but there is no zero in the total real amplitude and no sharp drop in the (averaged-amplitude) cross section for these cases. Well below the resonance region the separation of adjacent cross sections is seen to decrease for configurations with more $2p$ electrons, just as for the configurations with a fully filled K shell. This is again due to the decrease of the downward $2p \rightarrow 1s$ transition strength, defined per $2p$ electron, as the number of $2p$ electrons is increased, due to screening effects, combined with the replacement of outer-shell downward transitions with $2p$ downward transitions. The cross sections for configurations with four and five $2p$ electrons are again close together and are seen to cross over at low energy. (It should be remembered that the imaginary part of the amplitude, while small, is not negligible, and complicates the situation, especially when discussing such slight differences between cross sections.)

Figure 5 shows the differential cross section at forward angle for scattering from four different hollow-atom configurations, to see the types of differences which occur. (The angular dependence and the total cross section for scattering from hollow atoms and ions will be considered in Sec. V.) All cross sections approach the form-factor value at high energies from below, in contrast to the situation for configurations with a fully filled or partially filled K shell. Below the resonance region the cross sections are larger than the form-factor value, though the hollow-atom A1 cross section is close. One can see the position of resonances corresponding to downward transitions to the empty K shell shifting toward higher energies as the atom becomes more hollow, while the width narrows due to the weaker downward transitions from outer shells. The limiting value for downward transition resonance positions should be the Coulombic binding energy for a single electron in the $1s$ state, with $Z=6$. This is because, as the atom becomes more and more hollow, the electrons, now being placed in Rydberg states, see an increasingly Coulombic potential. Also, as the electrons become more loosely bound, their binding energy becomes insignificant when compared to the K-shell binding energy, so the transition energy, which is the difference between these, becomes closer to the K-shell binding energy, which itself is approaching the Coulombic value. There are no deep dips in the cross sections as the resonance region is approached from below. This is easily understood, since there is no canceling positive K-shell amplitude and hence no upward resonance transitions. The real amplitude is negative at low energy and becomes more and more negative as the resonance region is approached from below. Just above the resonance we see a dip in the cross section, though these dips are generally spurious for hollow-atom configurations with partially filled subshells, as seen for hollow lithium in Sec. VI.

The cross section for the hollow atom A1 is seen to be close to the form-factor value throughout the region, except at the position of the resonance, and at low energies, where the region of downward transitions to the L shell is being approached. The decrease in the magnitude of the negative real amplitude as the resonance is approached from above causes the cross section to fall. The other configurations in Fig. 5, involving $2p$ electrons, have elevated cross sections at forward angle below the resonance region. This enhancement is of particular interest since the cross section is not sharply forward peaked, and so there is a substantial total cross section, as will be discussed further in Sec. V. These cross sections are elevated due to the strength of the downward $2p \rightarrow 1s$ transition, and the corresponding step in the negative $L_{2,3}$-subshell real amplitude. However, it is not necessarily the case that the maximum cross section is obtained by placing all the electrons in the $2p$ state, since even though the number of the downward transitions is greatest, the strength of the transition per $2p$ electron decreases as the L shell is filled: cross sections for configurations with five and six $2p$ electrons are similar. At low energies these cross sections rise again, with the effect being more pronounced for configurations with more L-shell electrons. This is simply due to the increasing contribution of the imaginary amplitude f''. Since the K shell is vacant, the L shell is more tightly bound, and 100 eV is relatively closer to the L edge than for configurations involving K electrons.

V. ANGULAR DEPENDENCE AND TOTAL CROSS SECTIONS

Since the anomalous scattering factors are to a good approximation independent of angle at these energies, angular distributions may be understood in terms of the interplay of the form factor and the (angle-independent) anomalous amplitudes. The K-shell Coulombic form factor is easily found from Eq. (6):

$$f_K(q) = \frac{\left(\frac{Z}{2r_0}\right)^4}{\left[\left(\frac{Z}{2r_0}\right)^2 + q^2\right]^2}. \tag{10}$$

In general the form factor is equal to unity for zero momentum transfer, and drops to zero for large momentum transfer (q large in comparison with Z/r_0).

More specifically, the form-factor amplitudes for scattering off a particular bound electron will begin to fall off when the momentum transfer is close to the typical momentum of the bound electron; that is, when

$$\hbar q = 2\hbar\omega \sin\tfrac{1}{2}\theta \approx \sqrt{2\mu|E|}, \tag{11}$$

where E is the binding energy of the electron and μ is its reduced mass. Thus in C the K-shell form factor begins to show fall off at back angles for $\hbar\omega \approx 8$ keV, the L shell by ≈ 1.5 keV, and the N shell by ≈ 0.2 keV. For these low-Z cases the anomalous amplitudes for a given electron become small for energies well above its threshold, except in the vicinity of any of its strong downward transition energies, but for large q they may still dominate the form factor, which is dropping with q. As one passes through a strong resonance the real forward amplitude looks approximately like a step, as seen in Fig. 9. The magnitude of this step in f' is given by the strength of the transition in question. Below the threshold and Rydberg resonant region for a given electron the amplitude for scattering approaches zero. The contribution of the imaginary part of the total scattering amplitude to the scattering cross section can be important for energies just above threshold (it vanishes below threshold except at the positions of bound-bound transitions), but its contribution to the cross section falls off quickly with increasing energy. Knowing the binding energies of the electrons in a given configuration, and the anomalous scattering factors if they are significant, allows one to estimate how the cross section will drop as a function of angle or energy or both.

Since the below-threshold near-zeros, seen for configurations with two K electrons, involve the (inner) K-shell real amplitude cancelling with negative (near) form-factor amplitudes, we expect the position of the near-zero to change with angle if the form factors themselves fall off with increasing angle. Therefore, in our examples, if the configuration involves N-shell electrons, their negative form-factor contribution will decrease with increasing angle, causing the cancellation leading to the near-zero to occur at lower energies, further away from resonance. We find that for the configuration $(1s)^2(4s)^2(4p)^2$, for which the effect will be most apparent, the near-zero shifts to lower energy by ≈ 5 eV for backward angles (as compared to forward angles).

In Fig. 6 the cross sections at backward angle for hollow-atom and hollow-ion configurations (which differ only in having additional outer-shell electrons in the neutral atom) converge at high energy. This occurs because (except in the forward direction) the photon is no longer scattering off those outer electrons at high energies, and the scattering is off the same configuration of inner electrons. Near the K resonance region the cross sections for the hollow atom and the hollow ion differ, both due to the anomalous N-shell amplitudes and to the effects of fall off of the N-shell form factor, which is occurring through the K resonant region. For the ion the cross sections below the resonance region coincide for forward and backward angles. This is due to the fact that falloff in the amplitude has not occurred at these low energies for any of the electrons in the ion. For the atom, falloff in the amplitude for the loosely bound $4s$ electrons begins as the K resonance is approached, and the backward cross section starts to fall below the value at forward angle. The fact that the $4s$ electrons are contributing significantly to forward and backward scattering below the K resonance region explains why the cross sections are so different for the atom and the ion, while above the resonance region their contribution to backward scattering diminishes.

Figure 7 shows the scattering cross section as a function of angle at 1 and 5 keV for the ground state and an excited state with configuration $(1s)^1(2s)^2(2p)^2(4s)^1$. At 1 keV the cross section for the ground-state case is close to the $\propto(1+\cos^2\theta)$ angular behavior predicted by dipole approximation; and this is also true to a lesser extent for the excited case, reflecting that form factors have not yet begun to fall off. At 5 keV the cross section for the excited case is seen to fall more rapidly at first with angle, corresponding to a fall-off of the subshell amplitude for the electron in the $4s$ state. At larger angles the scattering from the L shell drops off. The cross section is lower for the excited state than for the ground state at larger angle because there is effectively one less electron to scatter from. At these energies scattering is still taking place from the whole of the K-shell charge distribution (twice as large for the ground state as for the excited state) at all angles. At back angles there is still some scattering from the L shell even at 5 keV.

For the energy range (100 eV to 10 keV) considered here, outer shells such as the N shell will have large forward amplitudes, even at 100 eV (still well above the N edge), but these will be strongly forward peaked in angle for energies in and above the K resonance region. Since the maximum of the peak stays constant as the energy is increased (as predicted by form-factor theory), this implies a small total cross section for the hollow atom A1, when integrated over all angles, as is seen in Fig. 8. For energies below and above the edge for a given shell (but not so high that the backward-angle momentum transfer is comparable to the typical electron momentum for that subshell: $\lesssim 8$, 1.5, and 0.2 keV for the K, L, and N shells, respectively) the amplitude will be essentially dipole in form, displaying the $\propto(1+\cos^2\theta)$ angular behavior in the cross section predicted by the Thomson formula. Referring back to Fig. 8, it was seen that the hollow atom C2 had a large forward cross section below the K-edge resonance region, in excess of the form-factor value and the corresponding cross section for the ground-state configuration. This is a dipole region for the L-shell amplitude, leading to the $\propto(1+\cos^2\theta)$ angular distribution in the cross section, thus giving rise to a very large total cross section, as much as five times as large as that for the ground state at 100 eV (just above the L edges). This is what is seen in Fig. 8. The total cross section for the hollow atom A1 falls off through the resonance region as the scattering amplitudes become forward peaked. The hollow atom C2 has a large total cross section below the resonance region, this being due to the dipole angular distribution and the large forward value for the differential cross section, as was discussed in Sec. IV.

As the K resonance region is approached from below, the ground-state total scattering cross section exhibits a deep minimum, while those for hollow-atom configurations do not, since there are no upward transitions. Just above the resonance region, the ground-state total scattering cross section is larger than that for the hollow atom C2 due to the contribution of the anomalous K-shell amplitudes. At higher energies, falloff in the L-shell amplitudes occurs, causing the K-shell contribution to dominate. In general hollow atoms (with the electrons in a given outer shell) will have large total cross sections for energies above the edge for that shell,

though at sufficiently high energies where the form factor is dropping off at finite angle, the total cross section will drop. [Thus, in our examples, above the L and K edges we have a large cross section for the hollow atoms, beginning to drop off for the hollow atom A1.] In addition, below the inner thresholds the cross section will be elevated due to the step in the real scattering amplitude associated with downward transitions to the (vacant) inner shells. [In our example, this enhances the hollow-atom C2 cross section in the region below the K edge. The step is much smaller for the $N \rightarrow K$ transition.]

VI. EFFECTS OF PARTIALLY FILLED SUBSHELLS

We have noted that the previous discussion was based on an averaging over all magnetic substates of a given subshell at the level of the scattering amplitude. This procedure (averaged-amplitude approach) is exact for fully filled subshells, but approximate for partially filled subshells. For ground-state atoms, one generally has a large fraction of the electrons in fully filled subshells, and this procedure is seen to work well [29]. However, with excited states there exists the possibility of there being greater effects associated with the approximate treatment of partially filled subshells. Note that only by using the averaged-amplitude approach was it possible to characterize general features solely in terms of the schematic amplitudes of Fig. 9. In the general case there will be other amplitudes. These concerns will be greatest for the lightest atoms, or for energies low enough that very few electrons participate in scattering.

A more proper treatment involves averaging the elastic scattering cross sections for all possible magnetic substate configurations, including incoherent elastic scattering, i.e. in which the magnetic substate configuration changes in scattering. In addition it may also be appropriate to consider inelastic scattering between nearly energy-degenerate subshells (e.g., $2p_{1/2}$ and $2p_{3/2}$), as this may not be distinguished from elastic scattering given a finite experimental energy resolution.

In Fig. 10 we show the forward-angle cross sections for scattering from a hollow lithium atom with a configuration $(2s)^2(2p)^1$, above and below the $L \rightarrow K$ resonance. The cross section in the averaged-amplitude approximation is shown together with the more proper elastic scattering cross section (averaging cross sections over all possible magnetic substate configurations). The total cross section includes both the elastic cross section (coherent and incoherent) and inelastic cross sections involving transitions between the (nearly energy-degenerate) $2p_{1/2}$ and $2p_{3/2}$ subshells. Effects associated with the averaging procedure will generally be comparatively larger than in carbon, as there are fewer electrons.

Generally the differences between the cross sections in Fig. 10 are fairly small, and generally they are expected to be less important than the (configuration-dependent) features seen in the carbon scattering cross sections using the averaged-amplitude approach. However, an important difference can be seen just above the resonance, where the averaged-amplitude approach leads to a near-zero in the cross section, which is removed in the more proper treatment, leaving only a dip in the cross section. The origin of this near-zero in the averaged amplitude approach is that the one real amplitude passes though zero as the resonance region is approached from above (see the L- and M-shell real amplitudes in Fig. 9), due to the presence of isolated downward transitions.

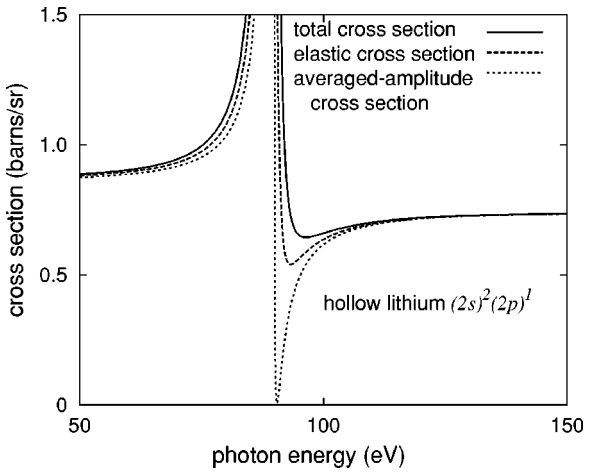

FIG. 10. Forward-angle cross sections for scattering from a hollow lithium atom with configuration $(2s)^2(2p)^1$ above and below the $L \rightarrow K$ resonance. The cross section in the averaged-amplitude approximation is shown together with the more proper elastic scattering cross section (averaging cross sections over all possible magnetic substate configurations). The total cross section includes both the elastic cross section (coherent and incoherent) and inelastic cross sections involving transitions between the (nearly energy-degenerate) $2p_{1/2}$ and $2p_{3/2}$ subshells.

However in the more proper treatment there are additional resonant elastic amplitudes, which are finite at this location, as well as finite resonant inelastic amplitudes corresponding to $2p_{1/2} \leftrightarrow 2p_{3/2}$ transitions. The corresponding cross sections should all be added incoherently. These additional cross sections (including incoherent elastic scattering and unresolved inelastic contributions) are generally large when the partially filled subshell anomalous amplitudes are large, and therefore they become unimportant away from resonances (except below the subshell's threshold), vanishing in the form-factor approximation. Therefore, a near-zero predicted in the averaged-amplitude approach will be spurious (i.e., filled in by the additional contributions) if it occurs sufficiently close to resonance. This is necessarily the case in Fig. 10, where it is the large anomalous real amplitude of the (partially filled) $2p$ subshell which gives rise to the averaged-amplitude near-zero. Therefore near-zeros above threshold (see Figs. 5 and 6) will generally be spurious except for the case of fully filled subshells [e.g., the $(2p)^6$ configuration in Fig. 5]. Since the L-shell amplitudes are still largely dipole dominated just above the resonance threshold, these features are expected to be similar at all angles.

Similarly below-threshold near-zeros will also generally be spurious if they occur sufficiently close to resonance, where the partially filled subshell anomalous amplitudes are large. However, as seen in Fig. 9, the K-shell real amplitude can be large and positive below the resonance where the $2p$

anomalous amplitude is small (the resonance in the $2p$ amplitude is comparatively narrow), such that the averaged-amplitude near-zero can occur at sufficiently low energy for the additional effects to be small, leading to a near-zero that is not spurious. Such is the case for the configurations with two K electrons in Fig. 3. For configurations with only one K electron (halving the positive below-resonance K-shell real amplitude) any near-zeros that occur are closer to resonance, and they are washed out by the additional effects. Note that for ground states of low-Z atoms, near-zeros generally occur far enough below threshold to be real effects in the cross section, at all angles. [For higher Z the relevant transition strengths, involving the valence electrons, are weaker, and there is a large form-factor background associated with many different subshells (and different corresponding falloffs), which complicates the situation.]

For configurations with two subshells that are half-filled, the averaged-amplitude approximation predicts that there will be no resonant contribution corresponding to transitions between the two subshells (since the upward transitions exactly cancel the downward transitions in the averaged amplitude). This leads to the averaged-amplitude cross section being smooth at the resonance position (and possibly then exhibiting a near-zero as the next resonance is approached, depending on the configuration). However there will generally be real resonant beyond-averaged-amplitude effects in the cross section, corresponding to transitions between the half-filled subshells.

VII. CONCLUSIONS

We have examined the differential and total cross section for elastic photon scattering from excited states of carbon atoms and ions, comparing results for different configurations including the ground-state configuration. Energies considered ranged from just above the L edge to well above the K edge, where form factors alone were found to be sufficient. Angle-dependent form factors, together with the anomalous scattering factors (taken to be angle independent), approximate well the scattering amplitudes over the whole energy range considered. The behavior of the full amplitudes and cross section can be understood in terms of the features of the subshell amplitudes.

Cross sections for configurations with the same number of K electrons (and the same number of total electrons) approached the high-energy form-factor limit along a common curve, giving rise to three such curves. Below the resonance region cross sections tended to separate according to the number of electrons in the subshells corresponding to the strongest transitions. For configurations with two K electrons (including the ground state) there were deep minima in the cross section below the resonance region. Cross sections for neutral atoms and ions, while different at forward angle due to the different number of electrons, were seen to coincide at backward angle for high energies if the configuration of the core electrons was the same.

Total integrated cross sections for hollow-atom configurations were investigated and compared to the ground-state configuration. Below the resonance region hollow atoms exhibited total cross sections substantially larger than that of the ground state by factors of 4 or 5 for configurations with all electrons present in the L shell. Above the resonance region the cross section for the hollow atom with all electrons present in the N shell fell quickly, while that for the hollow atom with all electrons present in the L shell remained comparable to the ground-state result.

The excited-state configurations considered here illustrate some of the dominant features in elastic photon scattering from excited atoms and ions for energies above and below the K resonance region, but above the L edge, while hydrogenic results suggest the behavior at valence-electron energies. The results presented here should provide some guidance in further discussing Rayleigh scattering from other multielectron excited atoms and ions and in other energy ranges.

The main results discussed here were obtained with the approximation of averaging over magnetic substates at the level of the scattering amplitude, exact only for closed subshells. Scattering from a hollow lithium atom, with and without making this approximation, was used to illustrate the further effects associated with partially filled subshells. Generally these effects are small, though it was seen that near-zeros in cross sections above the resonance region for hollow atoms are spurious, unless the dominant downward transitions are from fully filled subshells [the case of C $(2p)^6$].

ACKNOWLEDGMENTS

We wish to extend our thanks to C. David Shaffer for useful discussions. This work was supported in part by the National Science Foundation under Grant Nos. PHY-9601752 and PHY-9970293, and in part under the auspices of the U.S. Department of Energy by Lawrence Livermore National Laboratory under Contract No. W-7405-Eng-48.

[1] P. P. Kane, L. Kissel, R. H. Pratt, and S. C. Roy, Phys. Rep. **140**, 75 (1986).

[2] R. H. Pratt, L. Kissel, and P. M. Bergstrom, Jr., in *X-ray Anomalous (Resonance) Scattering: Theory and Experiment*, edited by K. Fischer, G. Materlik, and C. Sparks (Elsevier, Amsterdam, 1994), pp. 9–33.

[3] S. C. Roy, L. Kissel, and R. H. Pratt, Radiat. Phys. Chem. **56**, 3 (1999).

[4] H. Winter and F. Aumayr, J. Phys. B **32**, R39 (1999).

[5] N. Vaeck and J. E. Hansen, J. Phys. B **28**, 3523 (1995).

[6] Y. Azuma, S. Hasegawa, F. Koike, G. Kutluk, T. Nagata, E. Shigemasa, A. Yagishita, and I. A. Sellin, Phys. Rev. A **74**, 3768 (1995).

[7] E. Nardi, Z. Zinamon, D. Riley, and N. C. Woolsey, Phys. Rev. E **57**, 4693 (1998).

[8] R. F. G. Meulenbroeks, M. F. M. Steenbakkers, Z. Qing, M. C. M. van de Sanden, and D. C. Schram, Phys. Rev. E **49**, 2272 (1994).

[9] S. Maurmann and H.-J. Kunze, Phys. Fluids **26**, 1630 (1983).

[10] H. F. Doeble and K. Hirsch, Phys. Lett. A **54**, 267 (1975).

[11] H. Rohr, Z. Phys. **255**, 494 (1969).
[12] W. G. Wrobel, K. H. Steuer, and H. Rohr, Phys. Rev. Lett. **37**, 1218 (1976).
[13] M. Gavrila, Z. Phys. A **293**, 269 (1979).
[14] V. Florescu and A. Cionga, Z. Phys. A **321**, 187 (1985).
[15] M. Gavrila, Z. Phys. A **163**, 147 (1967).
[16] G. Basavaraju, L. Kissel, R. H. Pratt, J. C. Parker, S. C. Roy, and S. K. Sen Gupta, Phys. Rev. A **34**, 1905 (1986).
[17] S. L. Ionushauskas, A. V. Kuplyauskene, and Z. I. Kuplyauskis, Opt. Spektrosk, **47**, 447, (1979) [Opt. Spectrosc. **47**, 248 (1980)].
[18] Z. I. Kuplyauskis and A. V. Kuplyauskene, Opt. Spektrosk, **41**, 677 (1976) [Opt. Spectrosc. **41**, 399 (1976)].
[19] D. Salzmann and R. H. Pratt, Phys. Rev. A **30**, 2767 (1984).
[20] I. B. Goldberg and R. H. Pratt, Phys. Rev. A **36**, 2108 (1987).
[21] N. B. Avdonina, R. H. Pratt, and L. Chernysheva, in *The Physics of Highly Charged Ions*, edited by M. Stockli and P. Richard (AIP, New York, 1993), pp. 553–555.
[22] B. Rouvellou, J.-M. Bizau, D. Cubaynes, J. Novak, M. Pahler, L. Journel, F. J. Wuilleumier, L. VoKy, P. Faucher, A. Hibbert, and N. Berrah, Phys. Rev. Lett. **75**, 33 (1995).
[23] H. L. Zhou, S. T. Manson, L. VoKy, P. Faucher, F. Bely-Dubau, A. Hibbert, S. Diehl, D. Cubaynes, J.-M. Bizau, L. Journel, and F. J. Wuilleumier, Phys. Rev. A **59**, 462 (1999).
[24] D. Cubaynes, S. Diehl, L. Journel, B. Rouvellou, J.-M. Bizau, S. Al Moussalami, F. J. Wuilliumier, N. Berrah, L. VoKy, P. Faucher, A. Hibbert, C. Blancard, E. Kennedy, T. J. Morgan, J. Bozek, and A. S. Schlachter, Phys. Rev. Lett. **77**, 2194 (1996).
[25] S. Diehl, D. Cubaynes, J.-M. Bizau, L. Journel, B. Rouvellou, S. Al Moussalami, F. J. Wuilleumier, E. T. Kennedy, N. Berrah, C. Blanchard, T. J. Morgan, J. Bozek, A. S. Schlachter, L. VoKy, P. Faucher, and A. Hibbert, Phys. Rev. Lett. **76**, 3915 (1996).
[26] L. Journel, D. Cubaynes, J.-M. Bizau, S. Al Moussalami, B. Rouvellou, F. J. Wuilleumier, L. VoKy, P. Faucher, and A. Hibbert, Phys. Rev. Lett. **76**, 30 (1996).
[27] W. L. Glab and P. T. Glynn, Phys. Rev. A **58**, 4014 (1998).
[28] L. Kissel, Ph.D. thesis, University of Pittsburgh, 1977.
[29] J. P. J. Carney, R. H. Pratt, N. L. Manakov, and A. V. Meremianin, Phys. Rev. A **61**, 042704 (2000).
[30] J. P. J. Carney, Ph.D. thesis, University of Pittsburgh, 1999.
[31] L. M. Kiernan, M.-K. Lee, B. F. Sonntag, P. Sladeczek, P. Zimmermann, E. T. Kennedy, J.-P. Mosnier, and J. T. Costello, J. Phys. B **28**, L161 (1995).
[32] G. E. Brown, R. E. Peierls, and J. B. Woodward, Proc. R. Soc. London, Ser. A **227**, 51 (1955).
[33] W. R. Johnson and F. D. Feiock, Phys. Rev. **168**, 22 (1968).
[34] L. Kissel, R. H. Pratt, and S. C. Roy, Phys. Rev. A **22**, 1970 (1980).
[35] S. C. Roy, R. H. Pratt, and L. Kissel, Radiat. Phys. Chem. **41**, 725 (1993).
[36] M. Jung, R. W. Dunford, D. S. Gemmell, E. P. Kanter, B. Krässig, T. W. LeBrun, S. H. Southworth, L. Young, J. P. J. Carney, L. LaJohn, R. H. Pratt, and P. M. Bergstrom, Jr., Phys. Rev. Lett. **81**, 1596 (1998).
[37] E. W. B. Dias, H. S. Chakrabotty, P. C. Deshmukh, S. T. Manson, O. Hemmers, P. Glans, D. L. Hansen, S. B. Whitfield, D. W. Lindle, R. Wehlitz, J. C. Levin, I. A. Sellin, and R. C. C. Perera, Phys. Rev. Lett. **78**, 4553 (1997).
[38] E. G. Drukarev, N. B. Avdonina, and R. H. Pratt, Bull. Am. Phys. Soc. **44**, 132 (1999).
[39] In actuality, a modified form factor [W. Franz, Z. Phys. **98**, 314 (1936)] is used, which takes account of relativistic effects that are not important here.
[40] A. Costescu, P. M. Bergstrom, Jr., C. Dinu, and R. H. Pratt, Phys. Rev. A **50**, 1390 (1994).
[41] L. Kissel, B. Zhou, S. C. Roy, S. K. Sen Gupta, and R. H. Pratt, Acta Crystallogr., Sect. A: Found. Crystallogr. **51**, 271 (1995).
[42] P. M. Bergstrom, Jr., L. Kissel, R. H. Pratt, and A. Costescu, Acta Crystallogr., Sect. A: Found. Crystallogr. **53**, 7 (1997).